Aalborg Universitet

Power Oscillations Damping in DC Microgrids

Hamzeh, Mohsen; Ghafouri, Mohsen; Karimi, Houshang; Sheshyekani, Keyhan; Guerrero, Josep M.

Power Oscillations Damping in DC Microgrids

Mohsen Hamzeh, *Member, IEEE,* Mohsen Ghafouri, *Student Member, IEEE,* Houshang Karimi, *Senior Member, IEEE,* Keyhan Sheshyekani, *Senior Member, IEEE,* and Josep Guerrero, *Fellow, IEEE*

Abstract—This paper proposes a new control strategy for damping of power oscillations in a multi-source dc microgrid. A parallel combination of a fuel cell (FC), a photovoltaic (PV) system and a supercapacitor (SC) are used as a hybrid power conversion system (HPCS). The SC compensates for the slow transient response of the FC stack. The HPCS controller comprises a multi-loop voltage controller and a virtual impedance loop for power management. The virtual impedance loop uses a dynamic droop gain to actively damp the low-frequency oscillations of the power sharing control unit. The gain of virtual impedance loop is determined using small signal analysis and pole placement method. The Mesh analysis is employed to further study the stability of low-frequency modes of the overall dc microgrid. Moreover, based on the guardian map theorem, a robust stability analysis is carried out to determine a robustness margin for the closed-loop system. The main advantage of the proposed method is its robustness against uncertainties imposed by microgrid parameters. This feature provides DG units with plug-and-play capability without needing the exact values of microgrid parameters. The performance of the proposed control scheme is verified using hardware-in-the-loop (HIL) simulations carried out in OPAL-RT technologies.

Index Terms—DC microgrid, droop control, dynamic response, small signal analysis, virtual impedance loop.

I. Introduction

Existing passive electrical distribution systems are experiencing a compelling transition to active distribution networks with the ability of bidirectional electricity power exchange between the distribution systems and the main utility. This transition has been basically initiated by the employment of small scale distribution generation (DG) units and is being further facilitated by the advent of microgrids. Microgrids are the entities involving a number of DGs, energy storage systems (ESS) and loads that are electrically interconnected. This architecture has the capability to operate either as a grid-connected or as an islanded system, and offers a promising solution for coordinated control of an aggregation of DG units. A microgrid also helps with the efficient and reliable operation of the electrical networks, while improving the quality of service [1]–[3].

Generally, microgrids are categorized as ac, dc and hybrid ac-dc microgrids each providing particular benefits to the loads and the electrical network. AC microgrids have drawn an extensive attention on various aspects including interfacing converters, power sharing among parallel sources and power quality issues [4]–[6]. Despite their complex control topologies, ac microgrids are still popular since the existing power system is ac in nature.

The considerable amount of dc power generated by renewable energy sources, e.g., photovoltaic systems, fuel cells, and wind turbine systems, along with the rapid growth of dc loads are among the main driving factors for the development of dc microgrids. Moreover, dc microgrids require structurally simple power electronic interfaces and provide more efficient energy conversion systems as compared to the ac microgrids. The dc microgrids are also easier to control as they do not need any frequency and reactive power regulations. The dc converters can efficiently operate in parallel connection mode. Thus, the dc microgrids offer more modular and scalable system, and are more flexible to expand [7]–[10].

Despite their advantages, there are several technical challenges associated with the use of both ac and dc microgrids. Robust stability and dynamic performance of microgrid systems in both grid-connected and islanded mode of operation are among main technical challenges [11]–[13]. In the islanded mode, the control strategy has a more complicated structure as it must cope with voltage stability and power management among the DGs. Nevertheless, the DGs and ESSs must guarantee robust stability of the microgrid. The stability margin and the dynamic behavior of converter-based DG units in a dc system basically differ from those of conventional ac systems. Thus, further researches are required to overcome the challenges of dc microgrids [14], [15]. It should be noted that an appropriate coordinated power management among the hybrid energy resources in dc microgrids will maximize the microgrid robust stability margin.

Constant-power loads reduce voltage stability margin of dc microgrids, introduce significant oscillations, and even result in instability [16]. To overcome the instability issues caused by constant-power loads in dc distribution systems, various techniques have been proposed in the literature [17]–[19]. In particular, load shedding [20], filtering [21], direct connection of energy storage to the main bus [22], and control approaches [18] are among the well-known methods. The existing methods, however, do not investigate low-frequency instabilities (i.e., low-frequency power oscillations) in dc microgrids, imposed by power sharing control loops.

Virtual impedance loops are augmented to the control systems of inverters (mainly used in ac microgrids and UPS systems) for soft-starting of voltage source inverters [23], increasing the accuracy of real and reactive power sharing in microgrids [24], compensating voltage imbalance in islanded ac microgrids [25], and sharing harmonic and oscillatory currents in islanded microgrids [5], [26].

This paper presents a detailed modeling and control design

M. Hamzeh and K. Sheshyekani are with the Department of Electrical Engineering, Shahid Beheshti University, Tehran, Iran; M. Ghafouri and H. Karimi are with the Departement of Electrical Engineering, Polytechnique Montreal, QC, Canada; Josep Guerrero is with the Department of Energy Technology, Aalborg University, 9220 Aalborg, Denmark. e-mail: (mo_hamzeh@sbu.ac.ir, mohsen.ghafouri@polymtl.ca, houshang.karimi@polymtl.ca., k_sheshyekani@sbu.ac.ir, joz@et.aau.dk).

as well as an accurate robust stability analysis for HPCSs used by residential dc microgrids. The proposed control strategy employs an inductive virtual impedance loop to effectively damp the low-frequency power/current oscillations. The frequencies of the oscillations are usually lower than 300 rad/s (50 Hz) depending on the parameters of dc microgrid. The damping factor and frequency of oscillations are obtained using Mesh analysis approach. The overall dc microgrid is controlled based on a decentralized control strategy, i.e., each HPCS is individually controlled by a multi-functional control scheme. The SC energy storage systems are used to improve the transient response of the fuel cell (FC) stack and the PV modules. The proposed HPCS controller consists of a multi-loop voltage controller for regulating the microgrid voltage, and a virtual impedance loop for power management. The virtual inductive impedance loop (dynamic droop gain) improves the dynamic performance of the power sharing control unit. In this paper, using the guardian map theorem [27], a robust stability analysis is also performed to determine a robustness margin for the uncertain parameters due to the loads and lines. Finally, the performance of the dc microgrid is evaluated using hardware-in-the-loop (HIL) simulations carried out in OPAL-RT technologies. The HIL results confirm that the proposed control strategy effectively damps the low-frequency power oscillations, and properly performs power management among the energy sources and the storage units.

II. OPERATION PRINCIPLES OF PROPOSED CONTROL STRATEGY

The study system of this paper is a residential dc microgrid with the nominal voltage of 48 V, which is a standard value for these types of dc grids. Fig. 1 represents the general structure of a typical hybrid FC/PV/SC unit used to provide an almost constant dc-bus voltage for residential dc microgrids. The FC stack and the SC module are, respectively, connected to the dc microgrid through a unidirectional and a bidirectional dc/dc buck converter. The SC, as a fast and short term discharge ESS, plays an effective role for proper functionality of its corresponding DG unit in terms of power quality and reliability, particularly for the sensitive loads. The dc/dc converters are used to regulate the output voltage of each DG unit at the desired dc-link value, while providing a smooth output current. In this paper, we have used the exact models of FC and SC sources whose detailed descriptions are given in [28]. A PV system operating under maximum power point tracking (MPPT) conditions helps to minimize the fuel consumption of the FC module.

Fig. 2 shows the overall structure of the residential dc microgrid comprising four DGs, as labeled by DG$_1$, DG$_2$, DG$_3$ and DG$_4$. The first two units consist of an FC module working in parallel with an SC and a PV system. DG$_3$ is composed of an FC module equipped with an SC module, while DG$_4$ is a single PV system. The parameters of dc microgrid including the real powers, the line resistances and the parameters of the DG units are summarized in Table I.

The main objectives of the HPCS control system are as follows; (i) voltage control of the dc microgrid, (ii) power
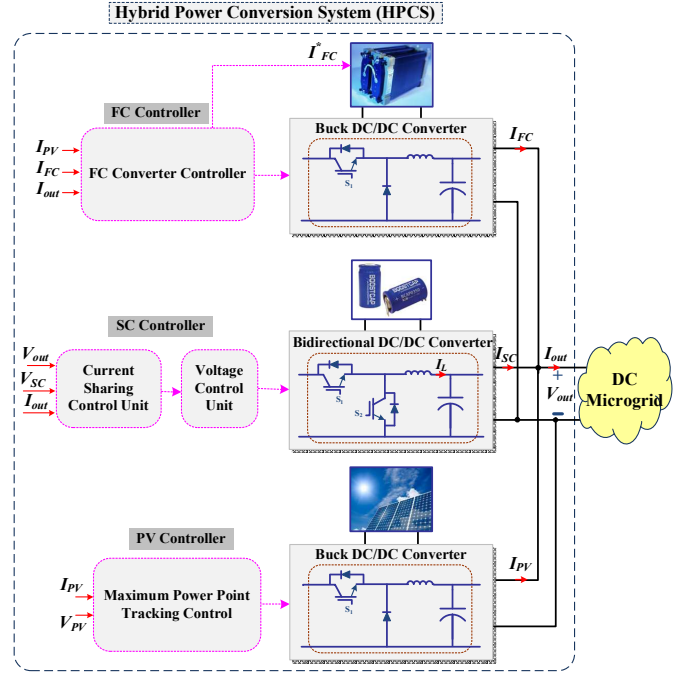
Fig. 1. General structure of an HPCS.

TABLE I
DC MICROGRID PARAMETERS

Parameter	Representation	Value
P_{base}	Base power	10 kW
P_{IC}	Interlink converter power	10 kW
V_{base}	DC microgrid voltage	48 V
HPCS Parameters		
$P_{FC1}, P_{PV1}, P_{SC1}$	Rated power of DG$_1$	2, 0.6, 2.2 kW
$P_{FC2}, P_{PV2}, P_{SC2}$	Rated power of DG$_2$	1, 0.8, 1.1 kW
P_{FC3}, P_{SC3}	Rated power of DG$_3$	0.5, 0.55 kW
P_{PV4}	Rated power of DG$_4$	0.8 kW
V_{PV}	MPPT voltage	70-150 V
V_{FC}	FC rated voltage	80 V
V_{SC}	SC rated voltage	55-65 V
f_{sw}	Switching frequency	25 kHz
L_f	SC inductor	2.5 mH
R_f	SC inductor resistance	0.01 Ω
C_f	SC converter capacitor	47 μF
Lines Parameters		
R_{L1}, R_{L2}, R_{L3}	Lines resistance	5, 15, 1 (mΩ)
R_{L4}, R_{L5}, R_{L6}	Lines resistance	1, 2, 1 (mΩ)
L_{L1}, L_{L2}, L_{L3}	Lines inductance	1, 3, 0.2 (μH)
L_{L4}, L_{L5}, L_{L6}	Lines inductance	0.2, 0.4, 0.4 (μH)

Fig. 2. Schematic diagram of DC microgrid consisting of four DG units.

Fig. 3. Structure of proposed control system for the SC converter.

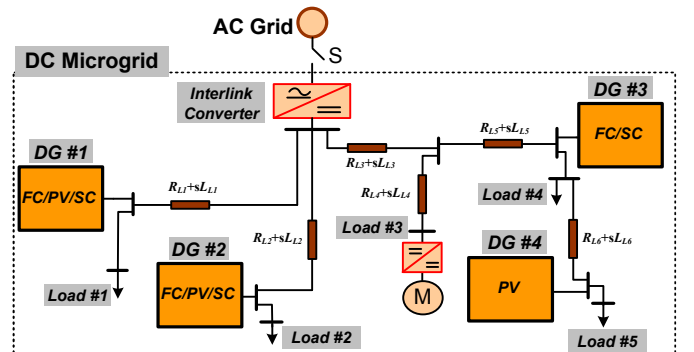management among the energy resources (FC, PV and SC) and the ESS of each single HPCS unit, and (iii) power sharing among all DG (HPCS) units to improve the dynamic performance of the dc microgrid. The controller of the FC converter is designed to regulate the hydrogen flow and the current of the FC module. Note that the unidirectional power flow of the FC converter decouples the dynamic of the FC and the SC converters [29]. In addition, the converter of the PV system is controlled such that the maximum power point tracking operating condition is fulfilled.

Fig. 3 shows the block diagram of the proposed control system employed by the buck converter of SC module. The control system consists of a voltage control unit, and a current sharing unit. The purpose of the voltage control unit is to regulate the voltage at each bus using a double-loop control system. The outer and the inner loops are used to control the output voltage and current, respectively. The reference value of the voltage controller is determined by the current sharing unit. As shown in Fig. 3, the current sharing unit is developed using a virtual impedance loop. The design procedure of the aforementioned units will be explained in the following subsections. It should be noted that the proposed strategy for power oscillations damping can be applied to any type of dc/dc converter with arbitrary topologies.

A. Voltage Controller Design

The voltage controller unit includes a proportional integral controller ($G_V(s)$) as the outer loop and a positive gain (K_c) as the inner loop. The inner loop is incorporated to increase the internal stability of the voltage controller loop and to protect the switches of the SC module converter against over current. Furthermore, the inner loop decreases the output impedance of the converter. The gain K_c is determined such that the damping factor and the overshoot of the dominant poles of the inner loop become 0.7 and %5, respectively. To eliminate the impact of the load dynamics, a feedforward controller is added in the voltage control loop.

The controller parameters of the outer loop are determined according to the desirable stability margins and appropriate bandwidth. To attain good robust stability margin, excellent noise immunity and fast transient response, a phase margin of 19 degrees and a bandwidth of 2 kHz are considered for the voltage controller. The designed controller whose parameters are given in Table II guarantees the above performance characteristics. The frequency response of the loop transfer function is illustrated in Fig. 4.

The block diagram of the proposed voltage controller is shown in Fig. 3. The output of the closed-loop system can be

Fig. 4. Bode plots of loop transfer function including the proposed controller.

TABLE II
PARAMETERS OF CONTROLLERS

Controller	Parameters Value
Voltage controller of SC converter	k_p=2, k_I=200
Current controller of SC converter	k_c=10
Current controller of FC Converter	k_p=0.05, k_I=0.25
Static droop coefficients of DGs	R_{D1}=0.057, R_{D2}=0.114, R_{D3}=0.228 Ω
Dynamic droop coefficients of DGs	L_{D1}=0.95, L_{D2}=1.25, L_{D3}=1.6 mH

expressed as

$$V_{out}(s) = H(s)V^*(s) - Z_{s0}(s)I_{sc}(s), \qquad (1)$$

where $V_{out}(s)$ and $I_{sc}(s)$ are the output voltage and output current of the SC converter, respectively, and the transfer functions $H(s)$ and $Z_{s0}(s)$ are obtained as

$$H(s) = \frac{V_{out}(s)}{V^*(s)}\Big|_{I_{sc}(s)=0} \qquad (2)$$

$$Z_{s0}(s) = -\frac{V_{out}(s)}{I_{sc}(s)}\Big|_{V^*(s)=0} \qquad (3)$$

The reference signal of the voltage loop, i.e., $V^*(s)$, is determined by the current sharing control unit.

B. Proposed Current Sharing Controller with Active Damping Capability (Virtual Impedance Loop)

To allow sufficient time-scale separation between the power and the voltage control loops, and to eliminate the ripples of DG output current, a first-order low-pass filter (LPF) with a

cutoff frequency (f_c) of 5 Hz is incorporated to the current sharing unit, as shown in Fig. 3. In other words, the use of LPF provides the voltage control loop with a ripple-free reference signal (V^*), which in turn results in a high quality voltage regulation. The high-frequency oscillations (ripples) imposed to the DG output currents are due to the switching ripples of the converter, power electronic-based loads, or even the oscillatory currents produced by some types of dc loads [26]. The cutoff frequency of the LPF is determined to eliminate the imposed ripples. It will be shown that the value of f_c has a significant effect on the low-frequency oscillations of DG output power. As shown in Fig. 3, the averaged current is then applied to the current sharing controller whose output is the reference signal of the voltage control loop. To achieve active damping of the low-frequency oscillations of DG output power, the following V-I droop function is proposed:

$$V^*(s) = V_0(s) - (R_D + sL_D)I_{avg}(s), \qquad (4)$$

where $V_0(s)$ is the nominal voltage of the dc microgrid, R_D and L_D are the static and dynamic droop gains (i.e., virtual impedance loop gains), respectively, and $I_{avg}(s)$ is the output of LPF. It should be noted that the conventional droop control strategy does not include any dynamic droop gain, i.e., L_D is zero. The static droop gain (R_D) is defined such that the output voltage of the converter (V_{out}) will not exceed the permissible voltage variations when the maximum power is transferred by the converter.

Using the small signal analysis, the value of L_D in (4) for each DG unit is determined such that an appropriate damping factor for low-frequency power sharing modes is achieved. The proposed dynamic term behaves as an inductive impedance which is implemented by a virtual impedance loop. To obtain L_D, first the characteristic equation of the current sharing unit will be derived. According to (1) and (4), the output voltage of the DG units can be calculated as:

$$V_{out}(s) = H(s)V_0(s) - Z_{s0}(s)I_{sc}(s) - [Z_{RD}(s) + Z_{LD}(s)]I_{out}(s), \qquad (5)$$

where $Z_{RD}(s)$ and $Z_{LD}(s)$ denote the output impedances of the HCPS units and are obtained in terms of the static and dynamic droop gains as follows:

$$Z_{RD}(s) = \frac{\omega_c R_D}{s + \omega_c}H(s), \text{ and } Z_{LD}(s) = \frac{s\omega_c L_D}{s + \omega_c}H(s). \quad (6)$$

According to Fig. 1, $I_{out}(s)$ in (5) is

$$I_{out}(s) = I_{sc}(s) + I_{pv}(s) + I_{FC}(s). \qquad (7)$$

From (5) and (7), the model of the closed-loop hybrid DG unit is derived as shown in Fig. 5. In Fig. 5, $H(s)V_0(s)$ and $Z_{s0}(s)$ are the voltage source and the output impedance of the SC converter, respectively, and the FC and PV systems have been modeled by two parallel current sources characterized by low transient responses. Moreover, the local load of each DG is modeled by a parallel resistance R_{load}, Fig. 5. The line resistance and inductance are respectively denoted by R_{Line} and L_{Line} which are unknown parameters, i.e., they may vary about their nominal values. $V_g(s)$ represents the Thevenin voltage of the rest parts of dc microgrid and its
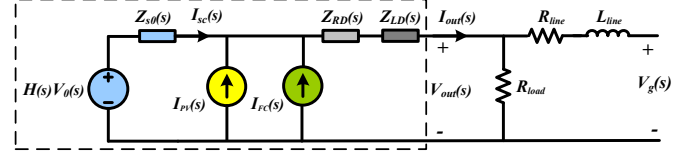

Fig. 5. Model of the closed-loop HPCS.

dynamic significantly depends on the dynamic behavior of the other DG units and line impedances. This will be detailed in the next subsection.

Based on Fig. 5, it can be concluded that

$$V_{out}(s) - V_g(s) = Z_{Line}(s)(I_{out}(s) - \frac{V_{out}(s)}{R_{load}}), \quad (8)$$

where $Z_{Line}(s) = R_{Line} + sL_{Line}$. The impact of the load resistance and line impedance on the low-frequency modes of the DG unit can be studied based on (5) and (8). Substituting (5) in (8) yields the output current of the DG as

$$I_{out}(s) =$$
$$\frac{(R_{load} + Z_{Line}(s))[H(s)V_0(s) + Z_{s0}(s)(I_{PV}(s) + I_{FC}(s))] - R_{load}V_g(s)}{R_{load}(Z_{Line}(s) + Z_{out}(s)) + Z_{out}(s)Z_{Line}(s)}, \qquad (9)$$

where $Z_{out}(s) = Z_{s0}(s) + Z_{RD}(s) + Z_{LD}(s)$. The denominator of (9) is the characteristic equation of the DG closed-loop system. Further, substituting (6) in (9) yields

$$(R_{load} + Z_{Line}(s))[(s + \omega_c)Z_{s0}(s) + \omega_c H(s)(R_D + sL_D)]$$
$$+ R_{load}(s + \omega_c)Z_{Line}(s) = 0. \qquad (10)$$

From (10), it can be concluded that the eigen-participation analysis of the DG system depends on the parameters of converters and controllers, line impedance, and load. In the first step of the analysis, DG$_1$ with R_{D1}=0.057 Ω and L_{D1}=0 is considered. Fig. 6 shows the loci of the dominant low-frequency modes of DG$_1$ when the line resistance (R_{Line}) increases from 0 to 0.1 pu, L_{Line}=0, and R_{load}=1.15 Ω. As it is observed, DG$_1$ system is unstable for $R_{Line} < 0.012$ pu. Moreover, the frequency of dominant low-frequency modes of DG$_1$ is between 110 to 150 rad/s (18 to 24 Hz) when the line resistance increases and, accordingly, the stability margin of the system improves. Theoretically, we can increase the line resistance to obtain an appropriate damping factor required for the stable operation of the microgrid. However, the increase of the line resistance is not always a practical solution as it increases the line losses and degrades the voltage profile. Moreover, it has a negative impact on the accuracy of the current sharing unit [7], [14]. Fig. 7 shows the impact of line inductance on the dynamic performance of dc microgrid for a specific line resistance (e.g., R_{Line}=0.0125 pu). As observed, the system with a higher line inductance presents a better damping factor.

As already discussed, the dynamic droop gain (L_D) is included to the current sharing controller to overcome the stability problem and to efficiently damp the low-frequency modes of the dc microgrid. The loci of the dominant low-frequency modes of DG$_1$, DG$_2$ and DG$_3$ for different values of L_D are shown in Fig. 8 (R_{Line} is assumed to be zero for all DG units). The dynamic droop gain L_D associated with
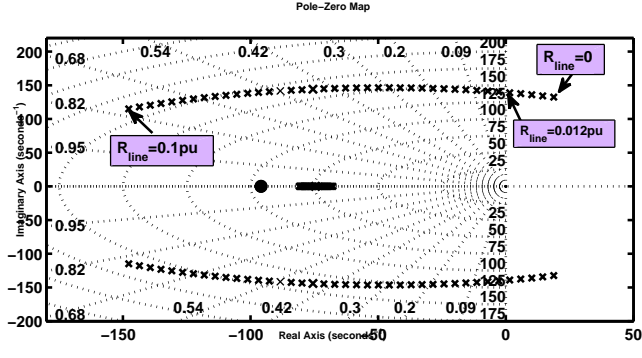
Fig. 6. Dominant low-frequency modes of DG_1 when R_{Line} changes from 0 to 0.1 pu.
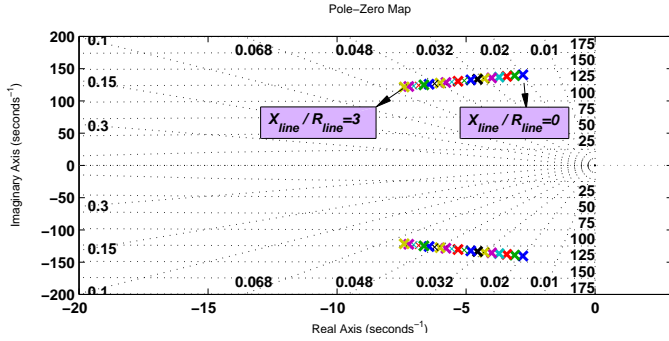

Fig. 7. Dominant low-frequency modes of DG_1 when R_{Line}=0.0125 pu and L_{Line} changes from 0 to 20 μH.

a specified static gain R_D is tuned such that the damping factor and the overshoot of the system become 0.7 and 5%, respectively. It should be noted that the dynamic droop gain L_D is adjusted for the worst operational condition, i.e., R_{Line}=0. Table II shows the controller coefficients designed for the DG units. It is to be noted that during design procedure of L_D for each DG unit, dynamics of the rest of dc microgrid are ignored, i.e., $V_g(s)$ in Fig. 5 is assumed constant. However, it will be shown that the damping factor of the overall dc microgrid will be very close to the desired damping factor of 0.7.
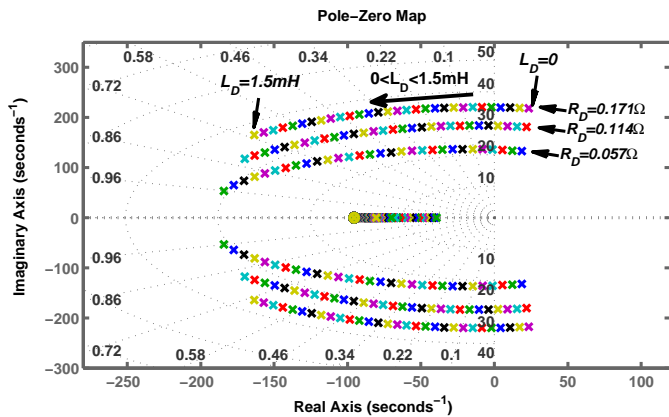
Fig. 8. Dominant low-frequency modes of DG units when L_D increases from 0 to 1.5 mH, and R_D=0.057 Ω for DG_1, 0.114 Ω for DG_2, and 0.228 Ω for DG_3.
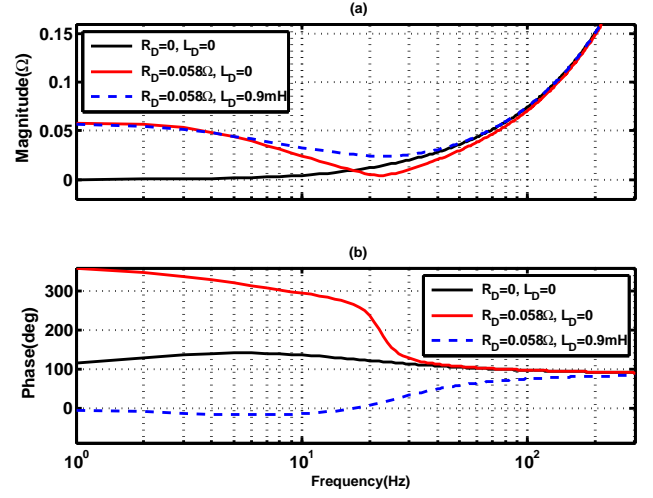
Fig. 9. Frequency response of the output impedance of the closed-loop subsystem DG_1 for three values of R_D and L_D.

Fig. 9 shows the frequency response of the output impedance, $Z_0(s)+Z_{RD}(s)+Z_{LD}(s)$, of DG_1 for three values of the static and dynamic droop gains. The output impedance of the DG units at low frequencies (e.g., $f < 5$ Hz) has significantly shifted by the static droop gain (R_D). As it is observed, the output impedance is increased for the frequencies between 5 Hz and 80 Hz when the virtual inductive impedance loop is incorporated in the conventional current sharing unit.

To investigate the impact of load power (or load resistance) on the stability of low-frequency modes of the DGs, the loci of these modes for DG_1 are depicted in Fig. 10, where the load power increases from 0 ($R_{load}=\infty$) to 5 kW ($R_{load}=0.46$ Ω). The analysis is performed for DG_1 for both conventional droop and proposed control systems when the line resistance is fixed at R_{Line}=0.0125 pu. The results show that, unlike the line resistance, the load resistance has a small impact on the damping factor and frequency of oscillations, and consequently on the stability of these modes.

Fig. 11 shows the dominant low-frequency modes of DG_1 when the cutoff frequency (f_c) of the LPF of the current sharing unit increases from 1 to 20 Hz, R_{Line}=0.0125 pu, and R_{load}=1.15 Ω. The analysis is performed for DG_1 for the two cases of conventional droop and the proposed control system. The results show that the cutoff frequency of the LPF has a significant effect on the damping factor and frequency of oscillations. It should be noted that although the increase in f_c improves the damping factor of the system, to eliminate the high-frequency ripples and oscillations of the DG unit output current, f_c should be kept less than 10 Hz.

C. Low-Frequency Stability Analysis of Overall dc Microgrid

To carry out a small signal analysis for the overall dc microgrid of Fig. 2, the linear models of all DG units including the lines and loads are obtained in the Laplace domain, as shown in Fig. 12, where $Z_{out_i}(s)=Z_{s0_i}(s)+Z_{RD_i}(s)+Z_{LD_i}(s)$ for each HPCS. The dominant low-frequency modes of the dc microgrid can be determined using its characteristic equation.
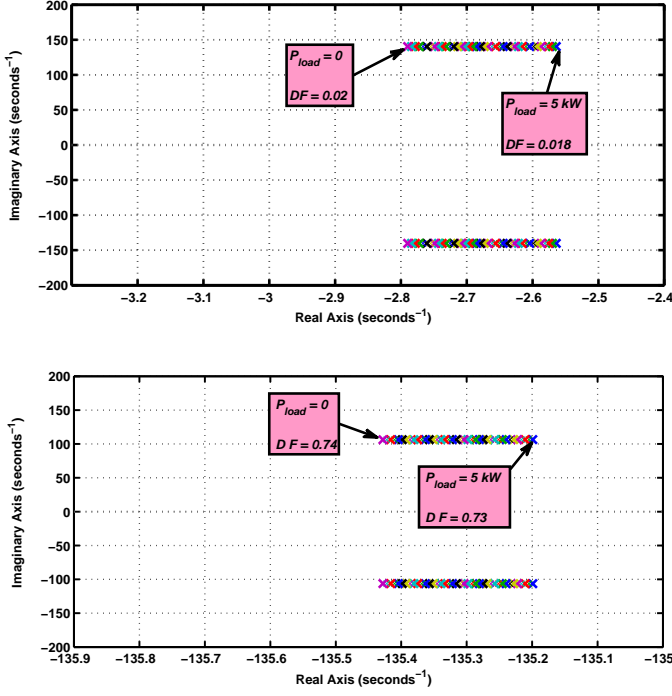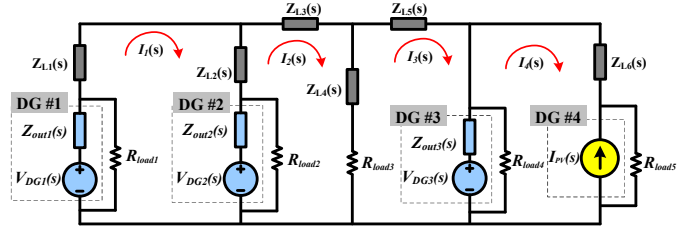
Fig. 12. The circuit model of the overall dc microgrid for mesh analysis.

The characteristic equation of a circuit is the determinant of its mesh impedance matrix. The mesh impedance matrix of Fig. 12 is denoted by $Z_{MG}(s)$ and can be expressed as:

$$\mathbf{Z_{MG}(s)} =$$

$$\begin{bmatrix} Z_{MG11}(s) & Z_{MG12}(s) & Z_{MG13}(s) & Z_{MG14}(s) \\ Z_{MG21}(s) & Z_{MG22}(s) & Z_{MG23}(s) & Z_{MG24}(s) \\ Z_{MG31}(s) & Z_{MG32}(s) & Z_{MG33}(s) & Z_{MG34}(s) \\ Z_{MG41}(s) & Z_{MG42}(s) & Z_{MG43}(s) & Z_{MG44}(s) \end{bmatrix},$$

(11)

where

$$Z_{MG11}(s) = Z_{out1}(s) \parallel R_{load1} + Z_{out2}(s) \parallel R_{load2}$$
$$+Z_{L1}(s) + Z_{L2}(s),$$
$$Z_{MG12}(s) = Z_{MG21}(s) = -[Z_{out2}(s) \parallel R_{load2} + Z_{L2}(s)],$$
$$Z_{MG13}(s) = Z_{MG31}(s) = Z_{MG14}(s) = Z_{MG41}(s) = 0,$$
$$Z_{MG22}(s) = Z_{out2}(s) \parallel R_{load2} + Z_{L2}(s) + Z_{L3}(s)$$
$$+Z_{L4}(s) + R_{load3},$$
$$Z_{MG23}(s) = Z_{MG32}(s) = -[Z_{L4}(s) + R_{load3}],$$
$$Z_{MG24}(s) = Z_{MG42}(s) = 0,$$
$$Z_{MG33}(s) = Z_{out3}(s) \parallel R_{load4} + Z_{L4}(s) + Z_{L5}(s) + R_{load3},$$
$$Z_{MG34}(s) = Z_{MG43}(s) = -[Z_{out3}(s) \parallel R_{load4}], and$$
$$Z_{MG44}(s) = Z_{out3}(s) \parallel R_{load4} + Z_{L6}(s) + R_{load5}.$$

(12)

Fig. 13 shows the dominant low-frequency modes of the dc microgrid for both cases of the conventional droop and the proposed control system. As it is observed, the damping factor of the dominant low-frequency modes is 0.015 when the conventional droop method is in service, whereas it is 0.774 (DF=0.774) when the proposed control system is used. It can be simply verified that the damping factor of the overall dc microgrid will be higher than 0.7 when the dynamic droop gain of each individual DG unit is adjusted such that its damping factor becomes 0.7. Fig. 13 also shows that the frequency of the dominant low-frequency modes is about 226 rad/s (36 Hz) when the DG units use the conventional droop controller. It is to be noted that the dominant low-frequency modes of the overall dc microgrid can not be determined by separately analyzing each single DG system.

III. ROBUST STABILITY ANALYSIS

In this section, based on the guardian map theorem presented in [27], a robust stability analysis is carried out to
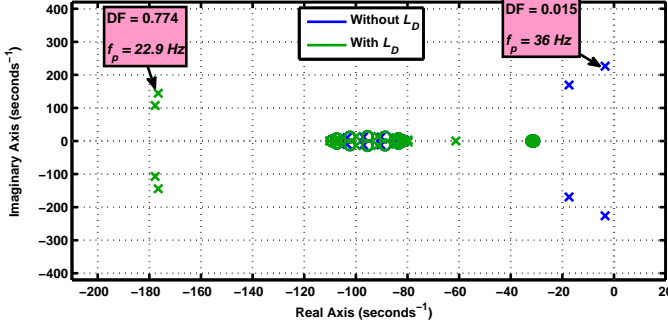

Fig. 10. Dominant low-frequency modes of DG$_1$ when the local load power increases from 0 to 5 kW, and R_{Line}=0.0125 pu. (Top) conventional droop is in service. (Bottom) proposed control system is in service.

Fig. 11. Dominant low-frequency modes of DG$_1$ when f_c increases from 1 to 20 Hz, and R_{Line}=0.0125 pu, P_{Load}=2 kW. (Top) conventional droop is in service. (Bottom) proposed control system is in service.

Fig. 13. Dominant low-frequency modes of dc microgrid with and without proposed control system.

Fig. 14. Guardian map analysis for the closed-loop polynomial with respect to parameters R_{line} and R_{load} in 3D space.

obtain a robustness margin for the uncertain parameters of dc microgrid. The characteristic equation of the closed-loop DG system, i.e., (10), includes the load and line parameters which are uncertain. In particular, the line and the load resistances (R_{line} and R_{load}) significantly vary about their nominal values, and thus affect robust stability and the dominant low-frequency modes of each closed-loop DG unit. On the other hand, the parameters of voltage controller, static droop gains, capacitor of buck converter, K_{PWM}, and LPF parameters are almost fixed or have very small variations. Therefore, we can assume that the parameters with small variations have no impact on the robust stability.

As discussed above, the two parameters R_{line} and R_{load} are the main sources of uncertainties in DG model. The robustness margin is a region in the space of parameters in which the closed-loop system remains stable. The guardian map is a powerful tool which accurately determines the robustness margin of an uncertain system. The main advantage of the guardian map is that it can be applied to any uncertain system irrespective of its structural complexity. A summary of guardian map is given in the following theorem and proposition [27].

Theorem 1. *Let $\mathscr{X}$ be the set of all polynomials with degree at most n, and let $\mathscr{S}$ be an open subset of $\mathscr{X}$. Moreover, assume that ν is a scalar valued function which maps $\mathscr{X}$ into complex numbers C. Then, ν guards $\mathscr{S}$ if*

$$x \in \delta\mathscr{S} \Leftrightarrow \upsilon(x) = 0, \qquad (13)$$

holds. In (13), $\delta\mathscr{S}$ denotes the boundary of region $\mathscr{S}$.

This theorem and its subsequent statement can be used to tackle the robust stability problem of parameterized family of polynomials [27].

Proposition 1. *Let $\mathscr{S}$ be guarded by the map ν and $r = (r_1, r_2, ..., r_k) \in U$ be the set of uncertain parameters. Moreover, assume that $x(r^0) \in \mathscr{S}$ for some $r^0 \in U$. Then:*

$$x(r) \in \mathscr{S} | \forall r \in U \Leftrightarrow \nu(x(r)) \neq 0 | \forall r \in U \qquad (14)$$

The above statement shows that for an arbitrary set in the s-plane, there exists a function which guards that given set. For example, the determinant function $\nu : A \to det(A)$ guards the set of nonsingular matrices $A_{n \times n}$.
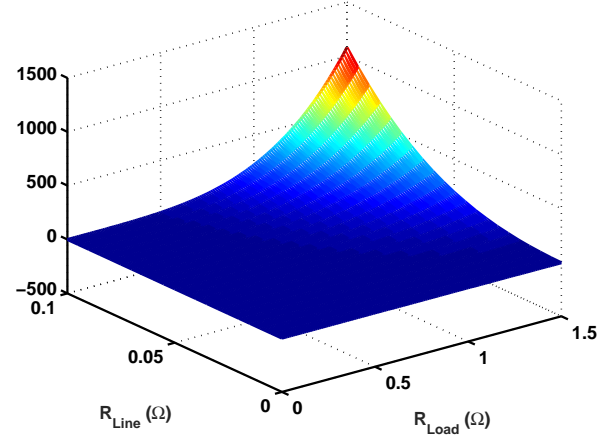
The set of polynomials given by (15) is stable in sense of Hurwitz if it is guarded by the function ν defined in (16), where $H(p)$ is the Hurwitz matrix associated with the polynomial $P(s)$ [30].

$$P(s) = a_n s^n + a_{n-1} s^{n-1} + ... + a_0 \qquad (15)$$

$$\nu : P \to det(H(p)) \qquad (16)$$

$$H(p) = \begin{pmatrix} a_{n-1} & a_{n-3} & a_{n-5} & . & . & . & 0 \\ a_n & a_{n-2} & a_{n-4} & . & . & . & . \\ 0 & a_{n-1} & a_{n-3} & . & . & . & . \\ . & a_n & a_{n-2} & . & . & . & . \\ . & . & . & . & . & . & 0 \\ . & . & . & . & a_3 & a_1 & 0 \\ 0 & 0 & . & . & . & a_2 & a_0 \end{pmatrix}$$

To apply the guardian map theorem to the closed-loop DG system, its characteristic polynomial is computed using (10) and Fig. 3. The Hurwitz matrix associated with the characteristic polynomial is then obtained. The guardian map is calculated and graphically depicted in three dimensional space, as shown in Fig. 14.

In order to determine the robustness margin, intersection of the guardian map surface depicted in Fig.14 with $\nu = 0$ (*xy*-plane) is obtained, as shown in Fig. 15. According to Fig. 15, the closed-loop DG system is robustly stable if the uncertain parameters R_{line} and R_{load} lie in the green region. Our simulation studies also confirm that the closed-loop DG system is robustly stable when the uncertain parameters are outside the red region.

IV. HARDWARE-IN-THE-LOOP SIMULATIONS

To demonstrate the effectiveness of the proposed control strategy, the microgird system of Fig. 2 is simulated using HIL RT-Lab of OPAL-RT technology. The HIL simulations are advantageous since they tackle the time inefficiency of the off-line simulations, and provide us with the possibility to
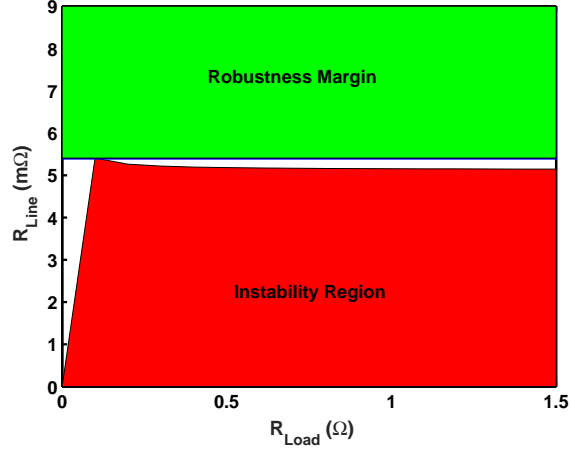
Fig. 15. Robustness margin (green region) of the closed-loop DG in R_{load}-R_{line} plane.

Fig. 16. Instantaneous currents of DC microgrid loads.

Fig. 17. Dynamic responses of DG units to the stepwise load increase at t=12 s: DG units output currents in (a) microgrid with low-impedance line when the conventional droop is used, (b) microgrid with high-impedance line when the conventional droop is used, and (c) microgrid with low-impedance line when the proposed control system is used.

make a sensitivity analysis on the system parameters. The dc microgrid is connected to the ac grid through an interlinking converter (IC). The power flow of the IC is zero indicating that the microgrid is in an islanded mode of operation. As discussed earlier, the dc microgrid contains four DG units whose building modules are described in Section II. DG$_1$, DG$_2$ and DG$_3$ are considered as dispatchable DG units having the capability to contribute to the power management of the microgrid. DG$_4$ is a single PV system and is considered as a non-dispatchable source. In this study, the loads are considered as a constant-impedance load. Load #3 is a dc motor which is connected to the dc microgrid via a boost dc/dc converter.

All DG units are equipped with the proposed PI controllers to regulate their buses voltages, while the proposed current sharing control method is employed to improve the transient response of the microgrid. The microgrid parameters are given in Tables I and II. Several load switchings are considered to verify the dynamic performance of the proposed control strategy. More specifically, the high-impedance line refers to the case in which the resistance of the microgrid lines are ten times higher than those of the low-impedance lines listed in Table I. To further accentuate the efficiency of the proposed method, the real-time simulations are repeated for the conventional droop strategy, i.e., only with static droop gains (V^*=V_0-$R_D I_{avg}$).

Initially, it is assumed that the current through the dc loads #1, #2, #3, #4 and #5 are 11, 12, 1, 16 and 9 A, respectively. At t=12 s, the load of dc motor (load #3) is suddenly increased such that its current becomes 58 A. Subsequent to this load change, at t=25 s, loads #1 and #4 are disconnected from the dc microgrid. The instantaneous currents of the dc loads are shown in Fig. 16.

Figs. 17 (a) and (b) show the dynamic responses of the DG units to the first load change, i.e., stepwise load increase, when the conventional droop is used for both cases of low- and high-impedance lines, respectively. To compare the results of the small signal analysis with those of real-time simulation, the dominant low-frequ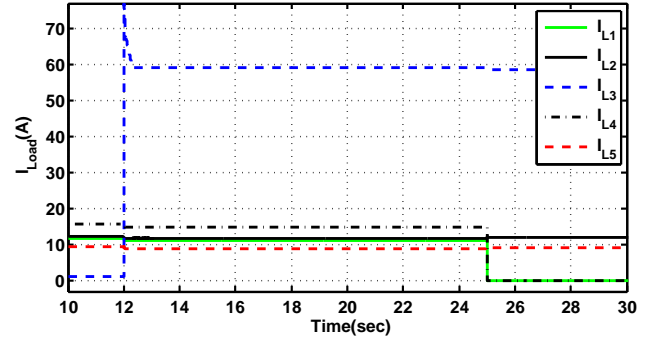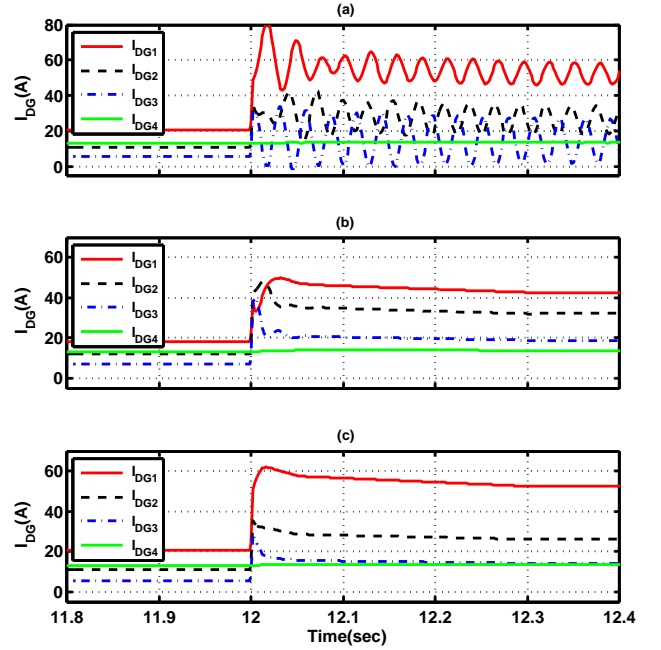ency modes of the dc microgrid employing the conventional droop method, i.e., L_D=0, for both low- and high-impedance lines are depicted in Fig. 18. As it is observed, the damping factor is 0.015 for the line with lower impedance, while it is 0.612 for dc microgrid with higher line impedance. Fig. 17 (a) shows that, for the case of low-impedance line with damping factor of 0.015, when the conventional droop strategy is adopted, the output currents of the dispatchable DG units experience significant oscillations with frequency of 36 Hz. This is due to the small damping factor of the dominant poles of the system with low-impedance lines. Fig. 18 also shows that the frequency of the oscillations of the dominant low-frequency modes for the microgrid with low-impedance line is about 36 Hz which matches with the simulation results, Fig. 17 (a).

For the same stepwise load increase, for the case of high-impedance lines, the current oscillations are considerably reduced which indicate the presence of a high damping factor,
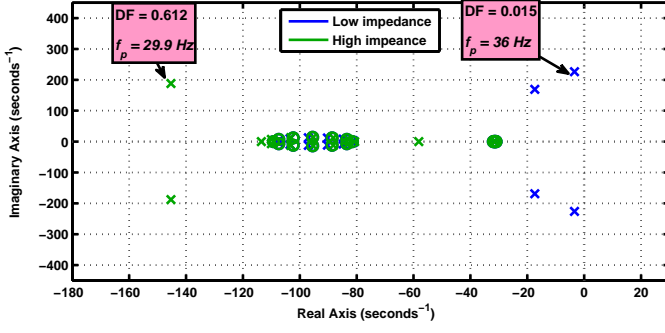
Fig. 18. Dominant low-frequency modes of dc microgrid employing conventional droop method, for both low- and high-impedance lines.

i.e., 0.612, as shown in Fig. 17 (b). Nevertheless, in the latter case, the current is not proportionally shared to the droop coefficients specified for each DG units, and the total loss is significantly increased. To overcome this problem, we resort to the proposed inductive virtual impedance loop that is expected to damp the low-frequency oscillations of the output current of the dispatchable DG units. This is confirmed for the case of the dc microgrid with low-impedance lines experiencing the same stepwise load increase (Fig. 17 (c)). As expected from the small signal analysis results of Fig. 13, the simulation results show that the proposed control strategy effectively damps (DF=0.774) the low frequency power oscillations due to the changes in the load. It should be noted that DG_4 is nondispatchable and cannot contribute to the microgrid power sharing.

Similarly, for the second load change (stepwise load decrease), the dynamic response of the DG units when the conventional droop is used for microgrid characterized by both low and high-impedance lines are respectively shown in Figs. 19 (a) and (b). As observed, for the case of low-impedance line, when the conventional droop strategy is used, the output currents of the dispatchable DG units are oscillatory due the small damping factor (0.015) of the dominant low-frequency modes of the system. However, for the same load step-down and for the case of high-impedance lines, the current oscillations are significantly damped due to the high damping factor characteristics of the lines (DF=0.612). Nevertheless, the high damping factor does not merely guarantee the appropriate current sharing among the units as shown Fig. 19 (b). Moreover, the use of inductive virtual impedance loop can effectively damp the unwanted oscillations in the HPCS units' output currents, while providing an appropriate current sharing among the dispatchable units. To achieve this goal, each unit decreases its current by drifting its reference voltage according to its V-I droop curve. A comparison between Figs. 19 (a) and (c) reveals the acceptable steady-state performance for both control strategies.

To further evaluate the performance of the proposed control strategy, similar load step-up, for the case of low-impedance lines with and without proposed virtual inductive loop, are applied at t=12 s. Fig. 20 shows the terminal voltage of DG_1. The microgrid voltage is changed according to the droop characteristics of the DG units. A comparison between
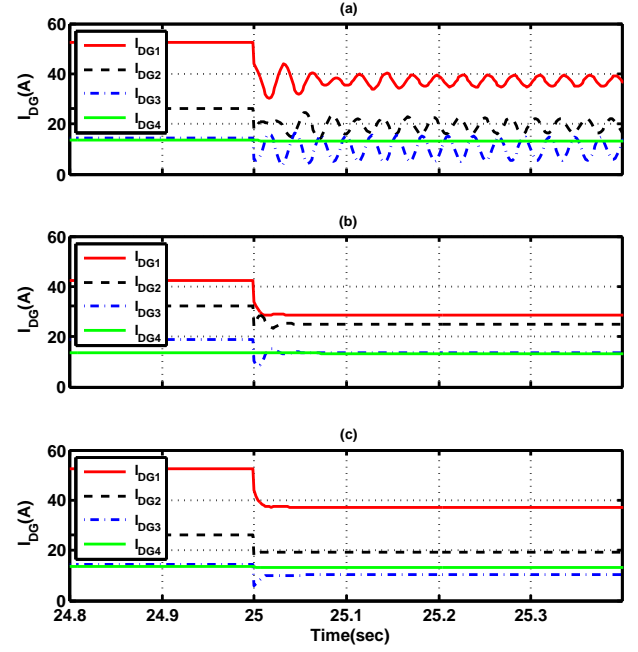

Fig. 19. Dynamic responses of DG units to the stepwise load decrease at t=25 s: DG units output currents in ((a) microgrid with low-impedance line when the conventional droop is used, (b) microgrid with high-impedance line when the conventional droop is used, and (c) microgrid with low-impedance line when the proposed control system is used.
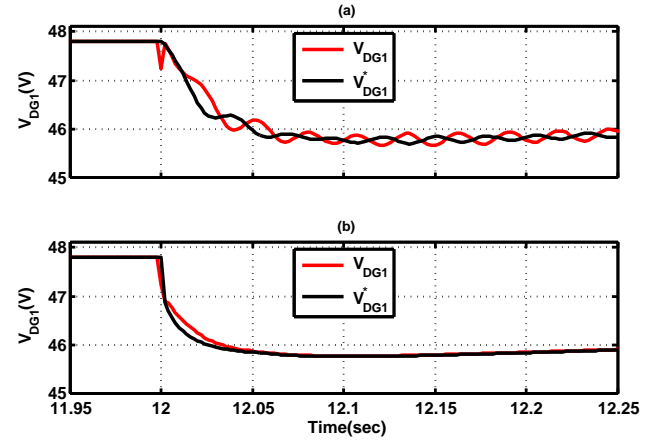

Fig. 20. Terminal voltage of DG_1 due to the stepwise load increase at t=12 s for microgrid with low-impedance lines, (a) conventional droop strategy, (b) proposed strategy.

the voltage profiles at the terminals of DG_1 obtained for the conventional and the proposed control strategies reveals that the proposed strategy succeeds to considerably reduce the low-frequency oscillations of the voltage during transient conditions.

In the final set of real-time simulations, for the microgrid with low-impedance line, subsequent to the same stepwise load change, the dynamic response of the FC/PV/SC modules of the DG units is shown in Fig. 21. As it is observed, the output currents of the PV modules remain constant. In fact, the PV system of each individual DG unit only contributes to provide a portion of the base demanded load, while each
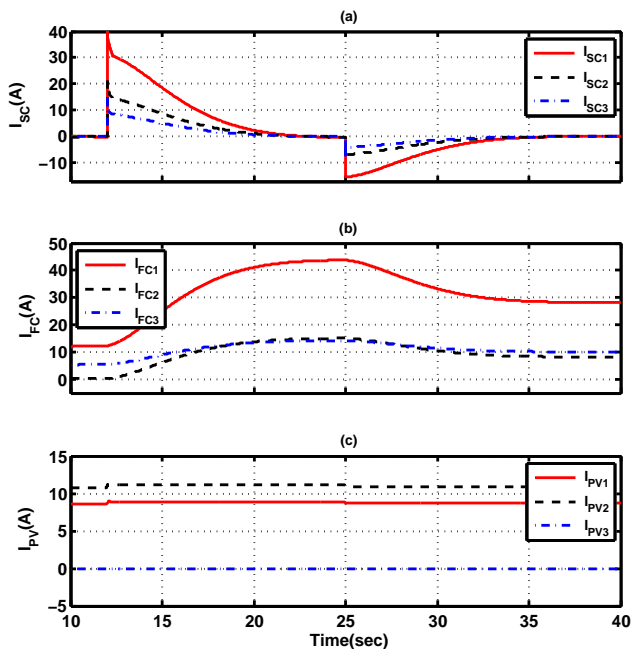
Fig. 21. Dynamic response of DG units to load changes: output current of (a) SC converters, (b) FC converters, and (c) PV converters of DG units.

DG unit participates in the power sharing according to the proposed current sharing strategy. To achieve this goal, at t=12 s, the FC module of each DG unit increases its output power to follow the reference current produced by the FC current controller, while the SC module of each DG unit compensates the shortage between the power of the FC system and the demanded load power. The FC system increases its output power at a limited response rate. It is to be noted that the SC modules will be in standby state when the FC modules successfully provide the demanded load power. Alternatively, at t=25 s when the microgrid is subjected to a load step down, the output current of the FC module converter is decreased to meet the new demanded load power. In this case, the surplus of the power generated by the FC modules is used to charge the SCs.

V. CONCLUSION

This paper presents a new control strategy for an HPCS to improve the dynamic response of a dc microgrid. The proposed control system employs a multi-loop voltage control system to regulate the microgrid voltage, and a virtual impedance loop to carry out efficient power management. Moreover, a supercapacitor (SC) energy storage is used to compensate the slow transient response of the fuel cell (FC) stack. It is shown that the low-frequency modes of microgrid are mainly dictated by the power management controllers. To actively damp the low-frequency current sharing modes, a virtual inductive impedance loop is proposed. The inductive gain of the dc source is determined using small signal analysis and pole placement methods. The proposed control strategy can simply be applied to other types of dc/dc converters with different topologies (e.g., isolated and non-isolated). In this paper, based on the guardian map theorem, a robust stability

analysis is also carried out to determine the robustness margin for the uncertain parameters of microgrid. The performance of the proposed control strategy is evaluated against both stepwise load increase/decrease using HIL RT-Lab simulator of OPAL-RT technologies. The HIL simulation results reveal that the proposed strategy:

- enhances the dynamic response of the dc microgrid during fast transients,
- effectively eliminates the low-frequency power oscillations,
- robustly regulates the microgrid voltage, and
- provides an appropriate power management among the energy sources and the storage unit of an individual HPCS.

REFERENCES

[1] R. Lasseter, "Microgrids," in *Proc. IEEE Power Eng. Soc. Winter Meeting*, pp. 305–308, 2002.
[2] F. Katiraei, R. Iravani, N. Hatziargyriou, and A. Dimeas, "Microgrids management," *IEEE power and energy mag.*, vol. 6, pp. 54–68, May. 2008.
[3] K. T. Tan, B. Sivaneasan, X. Y. Peng, and P. L. So, "Control and operation of a dc grid-based wind power generation system in a microgrid," *IEEE Transactions on Energy Conversion*, vol. PP, no. 99, pp. 1–10, 2015.
[4] J. He, Y. W. Li, R. Wang, and C. Zhang, "Analysis and mitigation of resonance propagation in grid-connected and islanding microgrids," *IEEE Transactions on Energy Conversion*, vol. 30, pp. 70–81, March 2015.
[5] M. Hamzeh, H. Karimi, and H. Mokhtari, "Harmonic and negative-sequence current control in an islanded multi-bus MV microgrid," *IEEE Trans. on Smart Grid*, vol. 5, pp. 167–176, Jan 2014.
[6] M. Hamzeh, H. Mokhtari, and H. Karimi, "A decentralized self-adjusting control strategy for reactive power management in an islanded multi-bus MV microgrid," *Canadian Journal of Electrical and Computer Engineering*, vol. 36, pp. 18–25, Winter 2013.
[7] H. Kakigano, Y. Miura, and T. Ise, "Configuration and control of a DC microgrid for residential houses," in *Transmission Distribution Conference Exposition Asia and Pacific, 2009*, pp. 1–4, Oct 2009.
[8] V. Nasirian, A. Davoudi, F. Lewis, and J. Guerrero, "Distributed adaptive droop control for DC distribution systems," *IEEE Transactions on Energy Conversion*, vol. 29, pp. 944–956, Dec 2014.
[9] Q. Shafiee, T. Dragicevic, J. Vasquez, and J. Guerrero, "Hierarchical control for multiple DC-microgrids clusters," *IEEE Transactions on Energy Conversion*, vol. 29, pp. 922–933, Dec 2014.
[10] J. Xiao, L. Setyawan, P. Wang, and C. Jin, "Power-capacity-based bus-voltage region partition and online droop coefficient tuning for real-time operation of dc microgrids," *IEEE Transactions on Energy Conversion*, vol. 30, pp. 1338–1347, Dec 2015.
[11] A. Radwan and Y.-R. Mohamed, "Linear active stabilization of converter-dominated dc microgrids," *IEEE Trans. on Smart Grid*, vol. 3, pp. 203–216, March 2012.
[12] S. Sanchez and M. Molinas, "Large signal stability analysis at the common coupling point of a DC microgrid: A grid impedance estimation approach based on a recursive method," *IEEE Transactions on Energy Conversion*, vol. 30, pp. 122–131, March 2015.
[13] M. Hamzeh, M. Ashourloo, and K. Sheshyekani, "Dynamic performance improvement of DC microgrids using virtual inductive impedance loop," in *Power Electronics, Drive Systems and Technologies Conference (PEDSTC), 2014 5th*, pp. 452–457, Feb 2014.
[14] D. Chen, L. Xu, and L. Yao, "DC voltage variation based autonomous control of DC microgrids," *IEEE Trans. on Power Del.*, vol. 28, pp. 637–648, April 2013.
[15] A. Khorsandi, M. Ashourloo, and H. Mokhtari, "A decentralized control method for a low-voltage DC microgrid," *IEEE Transactions on Energy Conversion*, vol. 29, pp. 793–801, Dec 2014.
[16] A. Kwasinski and C. Onwuchekwa, "Dynamic behavior and stabilization of DC microgrids with instantaneous constant power loads," *IEEE Transactions on Power Electronics*, vol. 26, pp. 822–834, March 2011.

[17] S. Sudhoff, K. Corzine, S. Glover, H. Hegner, and J. Robey, H.N., "DC link stabilized field oriented control of electric propulsion systems," *IEEE Transactions on Energy Conversion*, vol. 13, pp. 27–33, Mar 1998.

[18] M. Tabari and A. Yazdani, "Stability of a DC distribution system for power system integration of plug-in hybrid electric vehicles," *Smart Grid, IEEE Transactions on*, vol. 5, pp. 2564–2573, Sept 2014.

[19] A. Rahimi and A. Emadi, "Active damping in DC/DC power electronic converters: A novel method to overcome the problems of constant power loads," *IEEE Transactions on Industrial Electronics*, vol. 56, pp. 1428–1439, May 2009.

[20] R. Balog, W. Weaver, and P. Krein, "The load as an energy asset in a distributed DC smartgrid architecture," *IEEE Transactions on Smart Grid*, vol. 3, pp. 253–260, March 2012.

[21] P. Liutanakul, A. Awan, S. Pierfederici, B. Nahid Mobarakeh, and F. Meibodytabar, "Linear stabilization of a DC bus supplying a constant power load: A general design approach," *IEEE Transactions on Power Electronics*, vol. 25, pp. 475–488, Feb 2010.

[22] Y. S. Lee and G. T. Cheng, "Quasi-resonant zero current switching bidirectional converter for battery equalization applications," *IEEE Transactions on Power Electronics*, vol. 21, pp. 1213–1224, Sept 2006.

[23] J. M. Guerrero, L. G. de Vicuña, J. Matas, M. Castilla, and J. Miret, "A wireless controller to enhance dynamic performance of parallel inverters in distributed generation systems," *IEEE Transaction on Power Electronics*, vol. 9, pp. 1205–1213, Sept. 2004.

[24] J. M. Guerrero, L. G. de Vicuña, J. Matas, M. Castilla, and J. Miret, "Output impedance design of parallel-connected ups inverters with wireless load-sharing control," *IEE Transaction on Industrial Electronics*, vol. 52, pp. 1126–1135, Aug. 2005.

[25] J. M. Guerrero, J. Matas, L. G. de Vicuña, M. Castilla, and J. Miret, "Wireless-control strategy for parallel operation of distributed-generation inverters," *IEEE Transaction on Industrial Electronics*, vol. 53, pp. 1461–1470, Oct. 2006.

[26] M. Hamzeh, A. Ghazanfari, Y. A.-R. I. Mohamed, and Y. Karimi, "Modeling and design of an oscillatory current sharing control strategy in DC microgrids," *IEEE Trans. Ind. Electron.*, vol. 62, pp. 6647–6657, May 2015.

[27] A. Tits and L. Saydy, "On robust eigenvalue configuration," *Circuits and Systems, IEEE Transactions on*, vol. 38, pp. 138–139, Jan 1991.

[28] A. Ghazanfari, M. Hamzeh, H. Mokhtari, and H. Karimi, "Active power management of multihybrid fuel cell/supercapacitor power conversion system in a medium voltage microgrid," *IEEE Trans. on Smart Grid*, vol. 3, pp. 1903–1910, Dec. 2012.

[29] M. Hamzeh, A. Ghazanfari, H. Mokhtari, and H. Karimi, "Integrating hybrid power source into an islanded MV microgrid using CHB multilevel inverter under unbalanced and nonlinear load conditions," *IEEE Trans. on Energy Conver.*, vol. 28, pp. 643–651, Sep. 2013.

[30] B. R. Barmish, *New Tools for Robustness of Linear Systems*. Macmillan, 1993.

Mohsen Hamzeh (S'09-M'13) received the B.Sc. and M.Sc. degrees from the University of Tehran, Tehran, Iran, in 2006 and 2008, respectively, and the Ph.D. degree from Sharif University of Technology, Tehran, Iran, in 2012, all in electrical engineering. Since 2010, he has been the Senior Research Engineer with the SGP Company, Tehran, Iran. He joined the Department of Electrical and Computer Engineering, Shahid Beheshti University, Tehran, Iran, in 2013, where he is currently an Assistant Professor. His research interests include renewable energies, microgrid control and applications of power electronics in power distribution systems.

Mohsen Ghafouri (S'14) received the B.Sc. and M.Eng. degrees in electrical engineering from Sharif University of Technology, Tehran, Iran, in 2009 and 2011, respectively. He is currently pursuing his Ph.D. degree in electrical engineering at Polytechnique Montreal. His research interests include microgrid, wind energy, and application of robust control in power systems.

Houshang Karimi (S'03-M'07-SM'12) received the B.Sc. and M.Sc. degrees from Isfahan University of Technology, Isfahan, Iran, in 1994 and 2000, respectively, and the Ph.D. degree from the University of Toronto, Toronto, ON, Canada, in 2007, all in electrical engineering. He was a Visiting Researcher and a postdoctoral Fellow in the Department of Electrical and Computer Engineering, University of Toronto, from 2001 to 2003 and from 2007 to 2008, respectively. He was with the Department of Electrical Engineering, Sharif University of Technology, Tehran, Iran, from 2009 to 2012. From June 2012 to January 2013, he was a Visiting Researcher in the ePower lab of the Department of Electrical and Computer Engineering, Queens University, Kingston, ON, Canada. He joined the Department of Electrical Engineering, Polytechnique Montreal, QC, Canada, in 2013, where he is currently an Assistant Professor. His research interests include control systems, distributed generations, and microgrid control.

Keyhan Sheshyekani (M'10-SM'13) received the B.S. degree in electrical engineering from the University of Tehran, Tehran, Iran, in 2001, and the M.S. and Ph.D. degrees in electrical engineering from Amirkabir University of Technology (Tehran Polytechnique), Tehran, Iran in 2003 and 2008, respectively. He was with Ecole Polytechnique, Federale de Lausanne Lausanne (EPFL), Switzerland, in September 2007 as a Visiting Scientist and later as a Research Assistant. He is currently an Assistant Professor of electrical engineering with Shahid Beheshti University, Tehran. His research interests include power system modeling and simulation, smart grid, microgrids and electromagnetic compatibility.

Josep M. Guerrero (S'01-M'04-SM'08-FM'15) received the B.S. degree in telecommunications engineering, the M.S. degree in electronics engineering, and the Ph.D. degree in power electronics from the Technical University of Catalonia, Barcelona, in 1997, 2000 and 2003, respectively. Since 2011, he has been a Full Professor with the Department of Energy Technology, Aalborg University, Denmark, where he is responsible for the Microgrid Research Program. From 2012 he is a guest Professor at the Chinese Academy of Science and the Nanjing University of Aeronautics and Astronautics; from 2014 he is chair Professor in Shandong University; and from 2015 he is a distinguished guest Professor in Hunan University. His research interests is oriented to different microgrid aspects, including power electronics, distributed energy-storage systems, hierarchical and cooperative control, energy management systems, and optimization of microgrids and islanded minigrids; recently specially focused on maritime microgrids for electrical ships, vessels, ferries and seaports. Prof. Guerrero is an Associate Editor for the IEEE TRANSACTIONS ON POWER ELECTRONICS, the IEEE TRANSACTIONS ON INDUSTRIAL ELECTRONICS, and the IEEE Industrial Electronics Magazine, and an Editor for the IEEE TRANSACTIONS on SMART GRID and IEEE TRANSACTIONS on ENERGY CONVERSION. He has been Guest Editor of the IEEE TRANSACTIONS ON POWER ELECTRONICS Special Issues: Power Electronics for Wind Energy Conversion and Power Electronics for Microgrids; the IEEE TRANSACTIONS ON INDUSTRIAL ELECTRONICS Special Sections: Uninterruptible Power Supplies systems, Renewable Energy Systems, Distributed Generation and Microgrids, and Industrial Applications and Implementation Issues of the Kalman Filter; and the IEEE TRANSACTIONS on SMART GRID Special Issue on Smart DC Distribution Systems. He was the chair of the Renewable Energy Systems Technical Committee of the IEEE Industrial Electronics Society. He received the best paper award of the IEEE Transactions on Energy Conversion for the period 2014-2015. In 2014 and 2015 he was awarded by Thomson Reuters as Highly Cited Researcher, and in 2015 he was elevated as IEEE Fellow for his contributions on distributed power systems and microgrids.